Protein Science (1996), 5:729–741. Cambridge University Press. Printed in the USA.

4-Oxalocrotonate tautomerase, a 41-kDa homohexamer: Backbone and side-chain resonance assignments, solution secondary structure, and location of active site residues by heteronuclear NMR spectroscopy

JAMES T. STIVERS,[1] CHITRANANDA ABEYGUNAWARDANA,[1] CHRISTIAN P. WHITMAN,[2] AND ALBERT S. MILDVAN[1]

[1] Department of Biological Chemistry, The Johns Hopkins University School of Medicine, Baltimore, Maryland 21205-2185

[2] Medicinal Chemistry Division, College of Pharmacy, The University of Texas, Austin, Texas 78712-1074

(RECEIVED November 14, 1995; ACCEPTED January 9, 1996)

Abstract

4-Oxalocrotonate tautomerase (4-OT), a homohexamer consisting of 62 residues per subunit, catalyzes the isomerization of unsaturated α-keto acids using Pro-1 as a general base (Stivers et al., 1996a, 1996b). We report the backbone and side-chain ^{1}H, ^{15}N, and ^{13}C NMR assignments and the solution secondary structure for 4-OT using 2D and 3D homonuclear and heteronuclear NMR methods. The subunit secondary structure consists of an α-helix (residues 13–30), two β-strands (β_1, residues 2–8; β_2, residues 39–45), a β-hairpin (residues 50–57), two loops (I, residues 9–12; II, 34–38), and two turns (I, residues 30–33; II, 47–50). The remaining residues form coils. The β_1 strand is parallel to the β_2 strand of the same subunit on the basis of cross strand NH_i-NH_j NOEs in a 2D ^{15}N-edited ^{1}H-NOESY spectrum of hexameric 4-OT containing two ^{15}N-labeled subunits/hexamer. The β_1 strand is also antiparallel to another β_1 strand from an adjacent subunit forming a subunit interface. Because only three such pairwise interactions are possible, the hexamer is a trimer of dimers. The diffusion constant, determined by dynamic light scattering, and the rotational correlation time (14.5 ns) estimated from ^{15}N T_1/T_2 measurements, are consistent with the hexameric molecular weight of 41 kDa. Residue Phe-50 is in the active site on the basis of transferred NOEs to the bound partial substrate 2-oxo-1,6-hexanedioate. Modification of the general base, Pro-1, with the active site-directed irreversible inhibitor, 3-bromopyruvate, significantly alters the amide ^{15}N and NH chemical shifts of residues in the β-hairpin and in loop II, providing evidence that these regions change conformation when the active site is occupied.

Keywords: active site residues; NMR; structure

Reprint requests to: Albert S. Mildvan, Department of Biological Chemistry, The Johns Hopkins University School of Medicine, 725 N. Wolfe Street, Baltimore, Maryland 21205-2185.

Abbreviations: 2-HD, 2-oxo-1,6-hexanedioate; CT, constant time; DIPSI, decoupling in the presence of scalar interactions; FID, free induction decay; HSQC, heteronuclear single quantum correlation; HNCA, amide proton to nitrogen to α-carbon correlation; HNCACB, amide proton to nitrogen to α-carbon to β-carbon correlation; HNCO, amide proton to nitrogen to carbonyl correlation; MWCO, molecular weight cutoff; NOESY, nuclear overhauser effect spectroscopy; 2D, two-dimensional; 3D, three-dimensional; RF, radiofrequency; TOCSY, total correlation spectroscopy; TPPI, time-proportional phase incrementation; TSP, sodium 3-(trimethylsilyl)propionate-2,2,3,3,-d_4.

4-Oxalocrotonate tautomerase (E.C. 5.3.2) from *Pseudomonas putida mt-2*, is an enzyme involved in the bacterial catabolism of catechol to metabolites in the Krebs cycle (Bayley & Barbour, 1984). The enzyme catalyzes the isomerization of unconjugated α-keto acids, such as **1**, to the conjugated isomer **3** via a dienolic intermediate **2** (Fig. 1). The enzyme is a hexamer (Roper et al., 1994) with six identical subunits consisting of only 62 amino acid residues (Chen et al., 1992), giving a total molecular weight of 40,866. A 1.9-Å resolution crystal structure of a 73% homologous isozyme of 4-OT from *Pseudomonas* sp. CF600 (Subramanya et al., 1996) shows that the enzyme consists of a

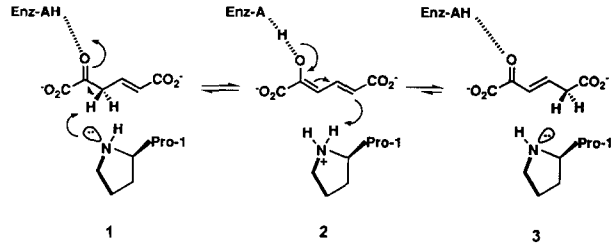

Fig. 1. Catalytic mechanism of 4-oxalocrotonate tautomerase (Stivers et al., 1996a, 1996b). Proline-1 ($pK_a = 6.4$), the general base, removes the 3-proton of substrate **1**, concerted with electrophilic catalysis at the C-2 oxygen atom by a putative enzymic general acid ($pK_a = 9.0$). For simplicity, the enolization is shown as concerted. The dienolic intermediate **2** is then reketonized and protonated stereospecifically at the 5-position to yield the *pro-[S]* enantiomer of **3** (Whitman et al., 1992).

trimeric arrangement of strongly interacting pairs of monomers, i.e., a trimer of dimers. However, the location of the active site was not established. Moreover, there are no solution structures available for either isozyme of 4-OT, or for any other keto-enol tautomerase. The small subunit size of 4-OT makes it an attractive model for studying the mechanism and structure of a keto-enol tautomerase in solution using heteronuclear NMR spectroscopy.

Recent NMR and mechanistic studies of 4-OT have established that the amino-terminal proline residue (Fig. 1) is the catalytic base (Stivers et al., 1996a, 1996b). A pK_a value of 6.4 for Pro-1 was determined by ^{15}N-NMR titration and this pK_a is 3 units lower than the model compound proline amide (Stivers et al., 1996a), most likely the result of an active site of low dielectric constant. The pH dependence of the reaction rate (Stivers et al., 1996a) also suggested a requirement for an enzymic general acid (AH, Fig. 1) with a pK_a of 9.0, to stabilize the developing negative charge on the carbonyl oxygen (Xue et al., 1990; Gerlt & Gassman, 1993).

The development of triple resonance multidimensional NMR spectroscopy has greatly extended the size limit of proteins accessible for structural determination by NMR methods (Bax & Grzesiek, 1993). These experiments, which rely on the transfer of magnetization through the heteronuclear scalar couplings, generally work well with proteins ≤30 kDa, with rotational correlation times $\tau_c \leq 10$ ns (Ikura et al., 1990b; Abeygunawardana et al., 1993, 1995; Fogh et al., 1994). However, the extension of these experiments to proteins that have higher molecular weights and $\tau_c \geq 10$ ns is difficult, mainly due to the short transverse relaxation times of the Cα nuclei. In these situations, the ^{13}Cα line widths approach the ^{1}H-^{13}C coupling constants, resulting in poor magnetization transfer efficiencies and low signal to noise ratios in some key experiments (Grzesiek et al., 1992; Yamazaki et al., 1994). Nevertheless, the solution structure of the p53 homotetramer (20 kDa, 42 residues/subunit) with a correlation time (14.8 ns) comparable to that of 4-OT (14.5 ns) has been solved (Clore et al., 1994, 1995; Clubb et al., 1995). Recently, it has been shown that fractional substitution of deuterons for protons attached to ^{13}C nuclei in uniformly ^{15}N- and ^{13}C-labeled proteins can significantly narrow the ^{13}C line widths and improve the magnetization transfer efficiencies (Yamazaki et al., 1994).

In this paper we report the complete backbone ^{1}H, ^{15}N, and ^{13}C sequence-specific assignments of 4-OT and ~90% of the ^{1}H and ^{13}C side-chain assignments based on a series of triple resonance multidimensional NMR experiments without resorting to ^{2}H labeling. The secondary structure of the 4-OT subunit, as well as the interactions comprising the dimer interface, were then derived from NOE and chemical shift data. In addition, transferred NOE studies with the bound partial substrate, 2-oxo-1,6-hexanedioate, and amide chemical shift changes upon chemical modification of Pro-1 with 3-bromopyruvate have suggested active site regions of 4-OT. A preliminary abstract of this work has been published (Stivers et al., 1995).

Results and discussion

^{1}H-^{15}N HSQC spectrum

The ^{1}H-^{15}N HSQC[1] spectrum of uniformly ^{15}N-labeled 4-OT (Fig. 2) shows 68 correlation peaks. Four peaks were sequence specifically assigned to the side-chain NH_2 groups of Gln-4 and Gln-15, based on 3D ^{15}N-NOESY-HSQC spectra (see below) in which these side-chain amide groups showed intraresidue NOEs to their own β and α-protons. Four other peaks, marked with asterisks in Figure 2, folded over from a more upfield region of the ^{15}N spectrum, were assigned to the side-chain N^{η}-H^{η} and N^{ϵ}-H^{ϵ} groups of two arginine residues based on the true ^{15}N chemical shifts for these resonances obtained from ^{1}H-^{15}N HSQC spectra using a larger ^{15}N spectral width (not shown). Furthermore, using a combination of ^{15}N-NOESY-HSQC, ^{15}N-TOCSY-HSQC, and HNCA experiments (see below), it was possible to unambiguously assign one pair of these side-chain correlations to Arg-29 (see below). The remaining set of N^{η}-H^{η} and N^{ϵ}-H^{ϵ} resonances could not be sequence specifically

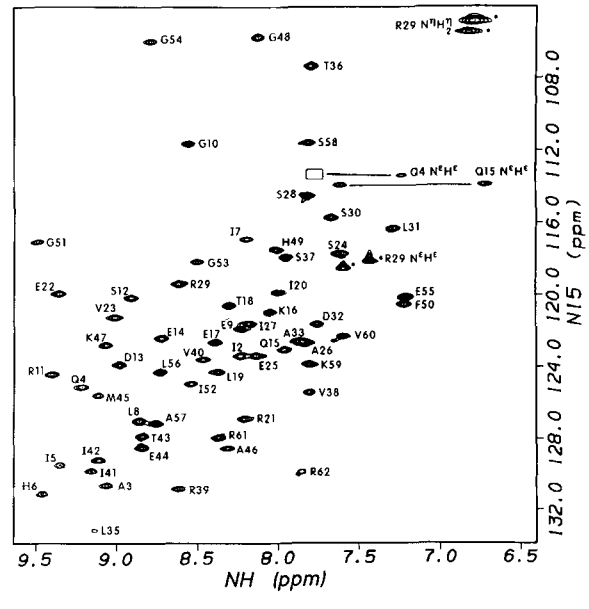

Fig. 2. Two-dimensional ^{1}H-^{15}N HSQC spectrum of uniformly ^{15}N-labeled 4-OT (6.0 mM subunits) recorded at 500 MHz proton frequency. Correlation peaks are labeled according to residue type and sequence number. The box indicates where the other Q4 $N^{\epsilon}H^{\epsilon}$ is seen at a two-fold lower contour level. Peaks labeled with an asterisk are folded over from side chain $N^{\epsilon}H$ and $N^{\eta}H$ of Arg residues (see text).

assigned, but belong to either Arg-11, Arg-21, or Arg-39 on the basis of the same 3D experiments listed above. The remaining major peaks are due to the expected 60 backbone amide resonances, taking into account that 4-OT contains one internal proline residue, and that the catalytic amino terminal proline is in fast exchange, consistent with its low pK_a value of 6.4 (Stivers et al., 1996a). The observation of only 60 major backbone amide resonances for the 4-OT hexamer demonstrates that each amide group is in an equivalent chemical environment in each subunit, indicating that the monomers are arranged symmetrically in the hexamer. Minor peaks, with intensities less than 5% of the major peaks, are associated with the resonances of the three carboxyl-terminal residues, Val-60, Arg-61, and Arg-62 (Fig. 2), indicating a small amount of conformational heterogeneity in this region.

Backbone resonance assignments

Three triple resonance experiments HNCACB (Fig. 3), HNCA, and HNCO (not shown) allowed the complete sequence-specific assignments of the backbone amide (^{15}N and NH), carbonyl, C_α, and C_β resonances. For Pro-1 and Pro-34, the ^{15}N resonance assignments were obtained from 1D ^{15}N spectra (Stivers et al., 1996b). The sequential C_α and C_β chemical shift values, which are quite diagnostic of amino acid type (Grzesiek & Bax, 1992), were then compared with the known primary sequence of 4-OT to rule out inconsistencies. Amide NH to H_α correlations obtained in a 3D ^{15}N-separated TOCSY-HSQC experiment with a 20.3-ms mixing time (not shown) provided Hα assignments for all residues except Pro-1 and Pro-34.

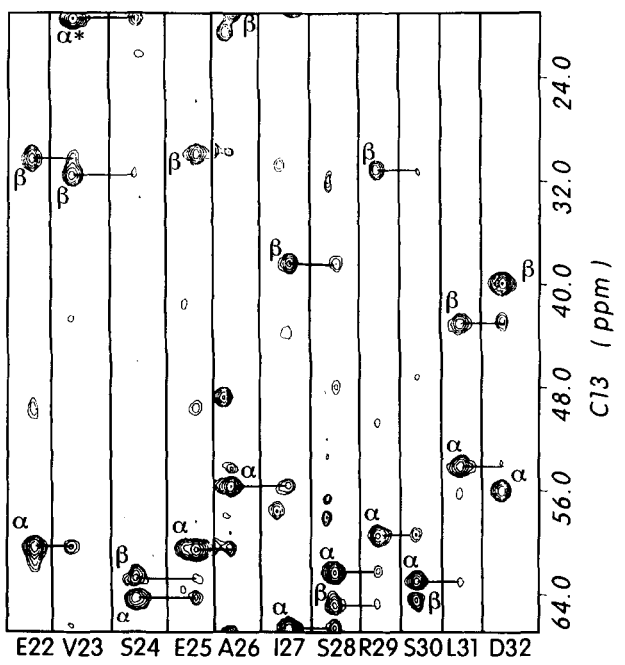

Fig. 3. Sequential strips extracted from the HNCACB experiment for residues Glu-22–Asp-32 of 4-OT (3.5 mM). Each strip represents a small region of the 2D plane taken at the ^{15}N frequency and centered at the HN frequency for each indicated residue. The C_β resonances were negative absorptive. Asterisk indicates that the C_α resonance of V23 was folded over from its true chemical shift.

The relatively high quality of the 3D HNCA (not shown) and 3D HNCACB spectra (Fig. 3), and the extent of the correlations that were seen may represent a favorable exception for a protein of this size. We attribute the high quality of these spectra to: (1) the compact spherical structure of the hexamer as seen in the crystal structure (Subramanya et al., 1996) and measured by dynamic light scattering measurements (see below); (2) the high concentrations of 4-OT used (3.5 mM subunits), and the absence of higher-order aggregates in the concentration range 0.3–7.9 mM subunits as determined by dynamic light scattering and NMR line width measurements; (3) the high stability of 4-OT, allowing relatively long acquisition times and high temperatures (42 °C) to be used; and (4) the simplified spectra resulting from the sixfold symmetry of the molecule. Thus, we conclude that, under favorable conditions, these NMR experiments may be applied successfully to molecules with the correlation time of 4-OT (see below).

Side-chain resonance assignments

A 3D HCCH-TOCSY experiment (not shown) yielded sequence-specific assignments of side-chain proton resonances and their attached ^{13}C resonances for nearly all the aliphatic amino acid residues except the H_β/C_β correlations of Glu-9, 14, 17, 22, 25, 44, and 55, which were assigned by 3D ^{15}N-NOESY-HSQC spectra and 2D NOESY spectra (Table 1). In addition, the weakness of the signal and/or spectral overlap precluded the assignment of the side-chain resonances of Ile-7 and Pro-34. The aromatic proton resonances of the single phenylalanine residue, Phe-50, and of the two histidine residues of 4-OT (His-6 and His-49) have been assigned previously using a combination of 2D NOESY and TOCSY spectra, as well as pH titration studies (Stivers et al., 1996a).

The hydroxyl proton resonances of Ser-24 and Ser-37 were also observed and assigned on the basis of: (1) a correlation peak between the hydroxyl proton and the H_β protons in a 2D TOCSY spectrum acquired in H_2O; (2) the disappearance of these peaks in spectra acquired in D_2O; and (3) a NOESY cross peak between the hydroxyl proton and its own amide NH resonance in 3D ^{15}N-NOESY-HSQC spectra.

Secondary structure determination

Because 4-OT is a symmetric hexamer, it is necessary to distinguish whether NOESY cross peaks originate from protons within a single subunit or from adjacent subunits. To resolve these ambiguities, and to determine the secondary structure of a single subunit, we used the following approach. First, a tentative secondary structure was assigned (independent of the NOE data) on the basis of the deviations of the Cα, Cβ, C′, and Hα chemical shifts from their random coil values (Spera & Bax, 1991; Wishart et al., 1992). Then, the sequential and near neighbor NN and αN NOE connectivities from a 3D ^{15}N-NOESY-HSQC spectrum (τ_{mix} = 50 ms, Fig. 4) were assigned tentatively as intrasubunit. To establish that the NN NOEs were indeed intrasubunit, both a 3D ^{15}N-HMQC-NOESY-HSQC experiment (not shown) and a 2D ^{15}N-double-edited ^{1}H-NOESY experiment (to improve sensitivity and resolve ambiguities) were performed

Table 1. *^{15}N, ^{13}C, and ^{1}H resonance assignments of 4-oxalocrotonate tautomerase at pH 6.5 and 42 °C*[a]

Residue	^{15}N	NH	C′	C^{α}	H^{α}	C^{β}	H^{β}	Others
1 Pro	49.2[b]	–	177.4	63.3	3.79[c]	34.9	1.83[c]	C^{γ} (28.2)[c], H^{γ} (1.67, 1.48)[c]; C^{δ} (48.7)[c], H^{δ} (2.81)[c]
2 Ile	123.42	8.20	174.3	60.3	5.04	41.7	1.76	C^{γ} (28.8), H^{γ} (1.59, 1.13); C^{δ} (14.9), H^{δ} (0.91); $C^{\gamma Me}$ (17.8), $H^{\gamma Me}$ (0.74)
3 Ala	130.60	9.07	175.2	49.9	5.65	23.1	1.11	
4 Gln	125.04	9.23	175.1	54.8	5.25	31.5	2.06, 1.68	C^{γ} (33.9), H^{γ} (1.99, 1.76); C^{δ} (172.7); N^{ϵ} (113.4), NH^{ϵ} (7.91, 7.22)
5 Ile	129.44	9.36	174.2	60.4	4.85	39.8	1.74	C^{γ} (27.3), H^{γ} (1.33, 0.83); C^{δ} (13.5), H^{δ} (0.59); $C^{\gamma Me}$ (18.5), $H^{\gamma Me}$ (0.63)
6 His	131.05	9.46	176.5	56.9	5.38	32.3	2.95, 2.81	H^{δ} (6.61); H^{ϵ} (7.36)
7 Ile	116.84	8.19	174.9	58.5	4.70	42.4	1.85	H^{γ} (1.29)[c]; C^{δ} (14.7)[c], H^{δ} (0.84)[c]; $C^{\gamma Me}$ (19.3)[c], $H^{\gamma Me}$ (0.64)[c]
8 Leu	127.01	8.88	179.1	56.1	4.46	43.8	1.61	C^{γ} (28.2), H^{γ} (1.62); $C^{\delta Me1}$ (25.6), $H^{\delta Me1}$ (1.02); $C^{\delta Me2}$ (24.8), $H^{\delta Me2}$ (0.98)
9 Glu	121.85	8.24	174.9	57.6	4.09	30.7	2.12, 2.05	C^{γ} (35.4), H^{γ} (2.35, 2.13)
10 Gly	111.53	8.56	176.2	45.7	3.66, 4.53			
11 Arg	124.36	9.41	177.3	55.5	4.71	31.0	1.84, 1.60	$C^{\gamma H}$ (2.19); C^{δ} (44.0), H^{δ} (3.28, 3.11)
12 Ser	120.10	8.92	175.8	57.7	4.57	66.5	4.06, 3.27	
13 Asp	123.84	8.99	179.5	58.6	4.35	40.3	2.82, 2.62	
14 Glu	122.34	8.73	180.0	60.8	4.14	29.9	2.10, 1.99	C^{γ} (36.8), H^{γ} (2.34)
15 Gln	123.09	7.96	179.2	60.2	4.06	29.6	1.86	H^{γ} (2.55, 2.44), C^{δ} (180.9); N^{ϵ} (113.85), NH^{ϵ} (7.61, 6.70)
16 Lys	120.96	8.05	178.2	61.6	3.69	32.0	1.69, 1.58	H^{γ} (0.97); H^{δ} (1.75); C^{ϵ} (41.9), H^{ϵ} (2.94, 2.55)
17 Glu	122.64	8.39	179.6	61.0	3.83	30.0	1.85, 1.68	C^{γ} (36.0), H^{γ} (2.32, 2.19)
18 Thr	120.54	8.30	175.4	67.8	3.85	68.9	4.36	C^{γ} (22.4), $H^{\gamma Me}$ (1.31)
19 Leu	124.28	8.37	178.7	59.0	4.12	42.1	2.28	C^{γ} (27.1), H^{γ} (1.27); $C^{\delta Me1}$ (26.1), $H^{\delta Me1}$ (0.93); $C^{\delta Me2}$ (26.8), $H^{\delta Me2}$ (0.82)
20 Ile	119.87	8.00	179.5	67.2	3.19	38.0	1.86	C^{γ} (31.0), H^{γ} (1.74); C^{δ} (13.4), H^{δ} (0.57); $C^{\gamma Me}$ (17.3), $H^{\gamma Me}$ (0.49)
21 Arg	126.90	8.21	178.8	61.6	3.98	30.7	2.00, 1.88	C^{γ} (27.4), H^{γ} (1.88); C^{δ} (43.3), H^{δ} (3.29)
22 Glu	119.83	9.36	181.9	60.3	4.02	30.2	1.73, 1.57	C^{γ} (36.9), H^{γ} (2.41, 2.32)
23 Val	121.16	9.02	177.7	67.5	3.47	31.5	2.08	$C^{\gamma Me1}$ (26.2), $H^{\gamma Me1}$ (0.88); $C^{\gamma Me2}$ (22.10), $H^{\gamma Me2}$ (0.70)
24 Ser	117.69	7.62	175.5	64.1	3.97	62.7	3.40	OH^{γ} (5.51)
25 Glu	123.35	8.14	178.5	60.5	3.92	30.0	2.01	C^{γ} (36.6), H^{γ} (2.44, 2.18)
26 Ala	122.70	7.83	181.3	55.7	4.04	19.2	1.32	
27 Ile	121.59	8.18	176.8	66.5	3.28	38.3	1.77	C^{γ} (30.0), H^{γ} (1.92); C^{δ} (14.6), H^{δ} (0.53); $C^{\gamma Me}$ (18.4), $H^{\gamma Me}$ (0.64)
28 Ser	114.43	7.81	178.1	62.2	4.12	64.6	3.87	
29 Arg	119.31	8.62	179.7	59.4	4.21	31.0	1.89, 1.82	C^{γ} (27.3), H^{γ} (1.66, 1.33); C^{δ} (43.8); H^{δ} (3.18), N^{ϵ} (86.85), NH^{ϵ} (7.59); N^{η} (73.37), NH^{η} (6.77)
30 Ser	115.66	7.67	174.4	62.9	4.18	64.4	3.60, 3.81	
31 Leu	116.30	7.31	176.6	54.0	4.33	43.0	1.47, 1.58	C^{γ} (26.2), H^{γ} (1.82); $C^{\delta Me1}$ (26.8), $H^{\delta Me1}$ (0.74); $C^{\delta Me2}$ (22.3), $H^{\delta Me2}$ (0.61)
32 Asp	121.63	7.76	175.2	55.9	4.29	39.8	3.05, 2.49	
33 Ala	122.57	7.87	–	48.8	4.92	20.6	1.02	
34 Pro	138.72	–	179.6	63.1	4.37[c]	34.3		
35 Leu	133.09	9.14	179.0	59.4	4.62	42.0	1.78	$C^{\delta Me1}$ (19.1), $H^{\delta Me1}$ (0.65); $C^{\delta Me2}$ (24.8), $H^{\delta Me2}$ (0.60)
36 Thr	107.30	7.79	175.6	64.5	3.87	69.4	4.31	$C^{\gamma Me}$ (22.5), $H^{\gamma Me}$ (1.28)
37 Ser	117.89	7.95	174.8	60.0	4.49	65.9	4.13, 3.93	OH^{γ} (5.05)
38 Val	125.49	7.79	177.7	64.2	4.34	32.9	2.13	$C^{\gamma Me1}$ (22.2), $H^{\gamma Me1}$ (0.91); $C^{\gamma Me2}$ (23.1), $H^{\gamma Me2}$ (0.82)
39 Arg	130.83	8.66	174.8	54.3	5.28	33.6	1.90, 1.72	C^{δ} (43.4), H^{δ} (3.26, 3.12)
40 Val	123.61	8.47	173.1	61.3	4.97	36.2	1.57	$C^{\gamma Me1}$ (23.0), $H^{\gamma Me1}$ (0.71); $C^{\gamma Me2}$ (22.8), $H^{\gamma Me2}$ (0.66)
41 Ile	129.82	9.17	175.8	61.2	4.75	43.4	1.45	C^{γ} (27.1), H^{γ} (1.23, 1.44); C^{δ} (13.5), H^{δ} (0.17); $C^{\gamma Me}$ (17.6), $H^{\gamma Me}$ (0.68)
42 Ile	129.15	9.12	175.2	60.9	4.53	39.3	1.54	C^{γ} (27.8), H^{γ} (1.36); C^{δ} (14.3), H^{δ} (0.77); $C^{\gamma Me}$ (17.3); $H^{\gamma Me}$ (0.32)
43 Thr	127.87	8.84	173.8	62.2	4.32	70.2	3.20	$C^{\gamma Me}$ (23.7), $H^{\gamma Me}$ (1.14)
44 Glu	128.51	8.85	176.3	55.9	4.86	32.9	1.86	C^{γ} (38.4), H^{γ} (1.86)
45 Met	125.52	9.12	175.6	54.4	4.87	35.5	1.91, 1.82	C^{γ} (30.5), H^{γ} (2.45, 2.33); C^{ϵ} (15.2), $H^{\epsilon Me}$ (0.84)
46 Ala	128.58	8.31	179.7	52.0	4.32	18.9	1.02	
47 Lys	122.75	9.08	178.3	60.7	4.09	32.7	1.69, 1.82	C^{γ} (25.9), H^{γ} (1.67, 1.49); C^{δ} (29.7), H^{δ} (1.69); C^{ϵ} (42.5), H^{ϵ} (3.00)
48 Gly	105.73	8.12	173.9	46.0	4.25, 3.67			
49 His	117.44	8.02	173.2	53.6	4.90	31.5	3.23	H^{δ} (6.58); H^{ϵ} (7.73)
50 Phe	120.56	7.21	174.2	55.0	5.95	42.6	3.24, 2.95	H^{δ} (7.32); H^{ϵ} (7.07); H^{ζ} (7.07)
51 Gly	116.95	9.51	172.6	45.3	4.76			
52 Ile	124.96	8.55	177.8	61.1	4.10	40.9	1.48	H^{γ} (1.80); C^{δ} (14.6), H^{δ} (0.83); $C^{\gamma Me}$ (17.6), $H^{\gamma Me}$ (0.69)
53 Gly	118.11	8.51	174.9	48.3	4.29, 3.72			
54 Gly	105.92	8.78	172.2	45.2	4.25, 3.22			
55 Glu	120.13	7.22	176.1	54.5	4.58	33.2	1.96, 1.81	C^{γ} (36.8), H^{γ} (2.17, 2.08)
56 Leu	124.38	8.74	179.6	55.9	4.52	43.4	1.66	C^{γ} (27.8), H^{γ} (1.81); $C^{\delta Me1}$ (26.2), $H^{\delta Me1}$ (0.92); $C^{\delta Me2}$ (24.6), $H^{\delta Me2}$ (0.84)
57 Ala	127.13	8.76	179.0	55.1	4.17	19.4	1.66	
58 Ser	111.53	7.81	175.3	59.1	4.28	63.8	3.98, 3.71	
59 Lys	123.86	7.81	176.8	57.1	4.38	34.0	1.93, 1.75	C^{γ} (25.2), H^{γ} (1.46, 1.33); C^{δ} (29.7), H^{δ} (1.68); C^{ϵ} (42.7), H^{ϵ} (2.95)
60 Val	122.33	7.60	176.3	63.2	4.06	33.4	2.03	$C^{\gamma Me1}$ (21.4), $H^{\gamma Me1}$ (0.94); $C^{\gamma Me2}$ (21.8), $H^{\gamma Me2}$ (0.91)
61 Arg	127.93	8.38	175.7	56.7	4.39	31.4	1.86, 1.75	C^{γ} (27.1), H^{γ} (1.64); C^{δ} (43.9), H^{δ} (3.20)
62 Arg	129.89	7.86	–	58.0	4.17	32.4	1.82, 1.69	C^{γ} (27.5), H^{γ} (1.57); C^{δ} (44.1), H^{δ} (3.17)

[a] ^{1}H and ^{13}C chemical shifts (ppm) are referenced to 3-(trimethylsilyl)propionate-2,2,3,3-d_4. ^{15}N chemical shifts (ppm) are referenced to liquid NH_3 (see text for details). Uncertainties in ^{15}N, ^{13}C, and ^{1}H chemical shift values are equal to or less than ±0.2, ±0.3, and ±0.05 ppm, respectively. Geminal methyls and geminal protons are numbered 1 and 2 based on downfield and upfield proton chemical shifts, respectively.

[b] The amino group of Pro-1 ($pK_a = 6.4$) titrates in this pH range. Limiting values for the ^{15}N chemical shift are 55.6 and 47.5 ppm at pH 4.92 and 8.77, respectively.

[c] Tentative assignments due to weak and/or overlapping resonances.

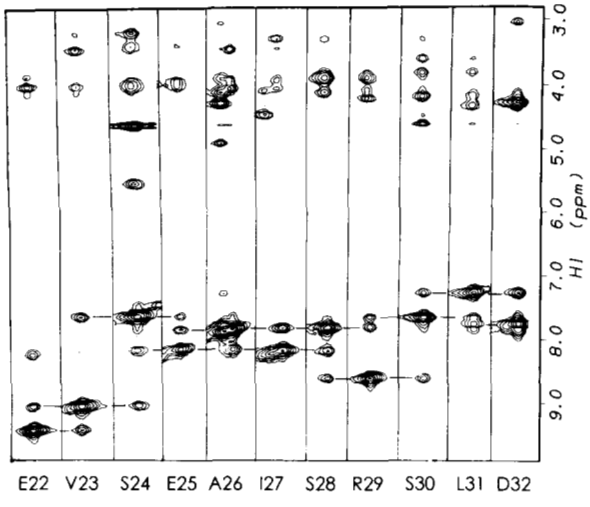

Fig. 4. Sequential strips extracted from the 3D ^{15}N-NOESY-HSQC experiment for residues Glu-22–Asp-32 of the α-helix of 4-OT. Each strip represents a small region of the 2D plane taken at the ^{15}N frequency and centered at the HN frequency for each indicated residue; NN (i, $i+1$) and NN (i, $i+2$) NOEs are indicated by horizontal lines.

using a 4-OT sample reconstituted with only two ^{15}N-labeled subunits/hexamer. In these experiments, statistically, only NOEs between ^{15}N-attached protons *within a single subunit* are observed.

These NOE data, summarized in Figure 5, are categorized as strong, medium, or weak after normalization of the cross peak heights with respect to those of the corresponding NH diagonal resonance to correct for NH peak height differences (Gagné et al., 1994). Evidence against significant spin-diffusion effects in the 50-ms NOESY spectra includes: (1) the absence of NN (i, $i+3$) correlations in the α-helical region (Fig. 4); and (2) αN (i, i)/αN ($i-1$, i) ratios that are significantly greater than 1 for residues in the α helix, and less than 1 for residues in β-sheet regions. This is significant because this ratio tends to approach unity as the amount of spin diffusion increases (Gagné et al., 1994).

The α-helix of 4-OT was identified by three criteria: (1) strong NN (i, $i+1$) NOEs, weak or absent αN (i, $i+1$) NOEs, and the presence of αN (i, $i+4$) NOE cross peaks (Wüthrich, 1986); (2) a series of upfield-shifted Hα and C$_\beta$ resonances (Spera & Bax, 1991; Wishart et al., 1992), downfield-shifted C$_\alpha$ and C′ resonances (Wishart et al., 1991); and (3) slow amide hydrogen exchange (Wüthrich, 1986). The β-strands were also identified by three criteria: (1) strong αN (i, $i+1$) NOEs and weak or absent NN (i, $i+1$) NOEs; (2) sequences of downfield-shifted H$_\alpha$ and C$_\beta$ resonances, and upfield-shifted C$_\alpha$ and C′ resonances (Spera & Bax, 1991; Wishart et al., 1992); and (3) slow hydrogen exchange patterns.

The data in Figure 5 unambiguously identify the location of one α-helix (residues 13–30), two β strands (β_1, residues 2–8, β_2, residues 39–45), two loops (residues 9–12, 34–38), two turns (residues 30–33, 47–50), and a β-hairpin (residues 50–57). The secondary structural components are described in detail below.

α-Helix

The beginning and end points, Asp-13 and Ser-30, of the 18-residue central helix (~5 turns) are well defined. An α-helix, rather than a 3_{10}-helix, is indicated by the presence of αN(i, $i+4$) connectivities (Wüthrich, 1986). A stretch of 11 consecutive, slowly exchanging amide NH resonances beginning at Leu-19 indicate hydrogen bonding and/or solvent inaccessibility. Inter-

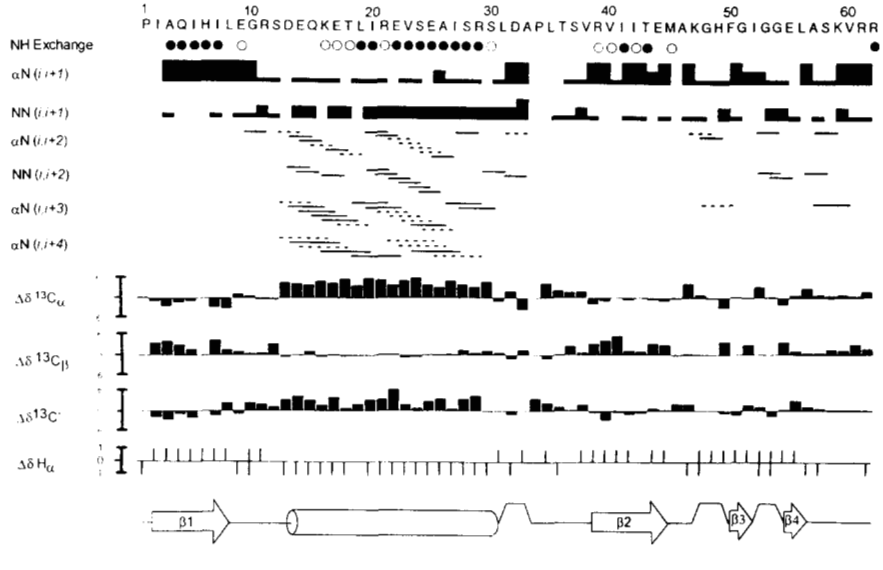

Fig. 5. Diagram of amide proton exchange rates, NOE connectivities, chemical shift differences from random coil values, and predicted secondary structure for the 4-OT subunit. The amide hydrogen exchange data ($T = 42$ °C) is divided into three classes: no circle, $t_{1/2} < 30$ min; open circle, 3 h $< t_{1/2} <$ 9 h; filled circle, $t_{1/2} \gg 64$ h. Exchange times intermediate between these limits were not seen. For the NOE data, the height of the bar indicates the strength of the NOE peak (strong, medium, weak). The chemical shift differences from the random coil values for each residue are illustrated utilizing the systems of Wishart et al. (1992) for Hα and ^{13}C′, and of Spera and Bax (1991) for ^{13}Cα and ^{13}Cβ.

estingly, Ser-24, which shows a slowly exchanging hydroxyl proton, is also located in this region. In contrast, the first three residues of the helix (13–15) show fast amide hydrogen exchange and strong amide cross peaks to water in the 3D ^{15}N-NOESY-HSQC spectrum, whereas the following three residues (16–18) show intermediate hydrogen exchange rates, suggesting fraying of the helix near its amino-terminal end, which allows solvent accessibility (Englander & Kallenbach, 1984; Spera et al., 1991).

β-Sheet

Two β-strands are identified in each monomer (Fig. 5). The β_1 strand (residues 2–8), which follows the catalytic proline, shows slow amide hydrogen exchange for the *consecutive* residues 3–7, and rapid exchange for the flanking residues Ile-2 and Leu-8. The β_2 strand (residues 39–45) shows *alternating* amide exchange rates for residues 41–43, intermediate exchange for residues Arg-39, Val-40, Ile-42, and Met-45, and fast exchange for Glu-44 (Fig. 5). These hydrogen exchange patterns indicate that the β_1 and β_2 strands are involved in a hydrogen bonded multistrand β-sheet structure and that one edge of the β_2 strand is exposed to solvent (Fig. 6).

The parallel arrangement of the β_1 and β_2 strands (Fig. 6) was indicated by the presence of 13 well-resolved cross strand NOEs observed in 2D NOESY spectra in ^2H_2O and in 3D ^{15}N-NOESY-HSQC spectra in H_2O. The weak cross strand NOEs were observed in NOESY spectra performed with mixing times of 50 and 100 ms, indicating them to be primary NOEs rather than spin diffusion artifacts. Protons in β_1 (residues 2–8) were found to give five long-range NN (i, j) and three αN (i, j) NOEs to protons in β_2, consistent with two parallel β-strands. Thus, the NOE data, together with the eight slowly exchanging amide protons in the parallel interface between the β_1 and β_2 strands, indicate up to eight possible hydrogen bonds in this interaction (Fig. 6).

To determine whether this parallel β_1-β_2 interaction was intra- or intersubunit, a 2D ^{15}N-double-edited-^{1}H-NOESY experiment (τ_{mix} = 75 ms) using a 4-OT sample reconsituted with two ^{15}N-labeled subunits per hexamer was performed (see the Materials and methods). In this experiment, statistically, only NOEs between ^{15}N-attached protons *within a single subunit* are observed. Because of the weak intensities of these NOEs due to the large cross strand distances (~4 Å), the 2D NOESY experiment was performed so that the signal/noise ratio could be maximized. Slices from this 2D spectrum (Fig. 7A, B) show four of the expected five long-range NN(i, j) NOEs between the β_1 and β_2 strands that were seen with the uniformly ^{15}N-labeled enzyme sample. For comparison, shown in Figure 7C is a slice though the amide proton chemical shift of Arg-29 showing the strong NN ($i, i + 1$) and NN($i, i - 1$) NOEs (r = 2.8 Å) and the weaker NN ($i, i - 2$) NOEs (r = 4.2 Å), as expected for a helical region. Finally, as an important negative control, the HN_i-HN_j intersubunit β_1-β_1 NOE between His-6 and Ile-2 that was seen in the 3D ^{15}N-NOESY-HSQC spectrum of the fully ^{15}N-labeled enzyme sample was not seen in this spectrum, confirming that NOEs within isolated subunits are being observed (data not shown). Hence, this experiment establishes the parallel β_1-β_2 interaction to be within a single subunit.

Protons from β_1 (residues 2–6) also showed five long-range NOEs to protons of a β_1 strand from a second subunit, including two strong $\alpha\alpha(i, j)$ NOEs (Fig. 6). These long-range NOEs, and the slowly exchanging amide protons of Gln-4 and His-6 from the β_1 strands of two adjacent subunits, are consistent with an antiparallel alignment of these strands, and show unambiguously that this interaction constitutes a subunit interface.

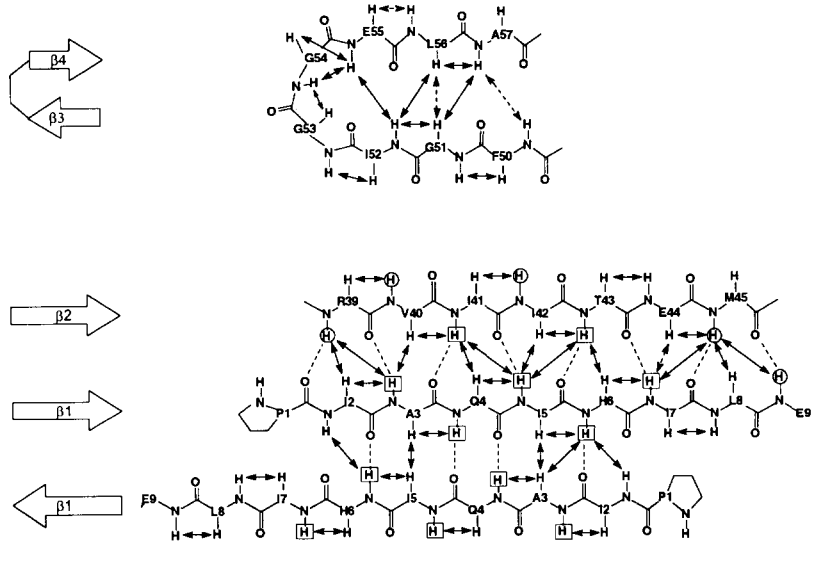

Fig. 6. Diagram of the β-sheet structures for 4-OT. Solid lines indicate the long-range HN_i-HN_j, HN_i-$H\alpha_j$, and $H\alpha_i$-$H\alpha_j$ NOESY correlations observed in 3D NOESY-HSQC and 2D NOESY spectra. The β_1-β_2, as well as the β-hairpin HN_i-HN_j interactions were shown to be intrasubunit on the basis of the 2D ^{15}N-double-edited ^{1}H-NOESY spectrum of 4-OT with two ^{15}N-labeled subunits/hexamer (Fig. 7); the β_1-β_1 interaction is across a dimer interface. Dotted lines show hydrogen bonding patterns inferred from slow amide hydrogen exchange (squares) and the observed long-range NOEs. Open circles indicate amide protons that have intermediate exchange rates (see Fig. 5).

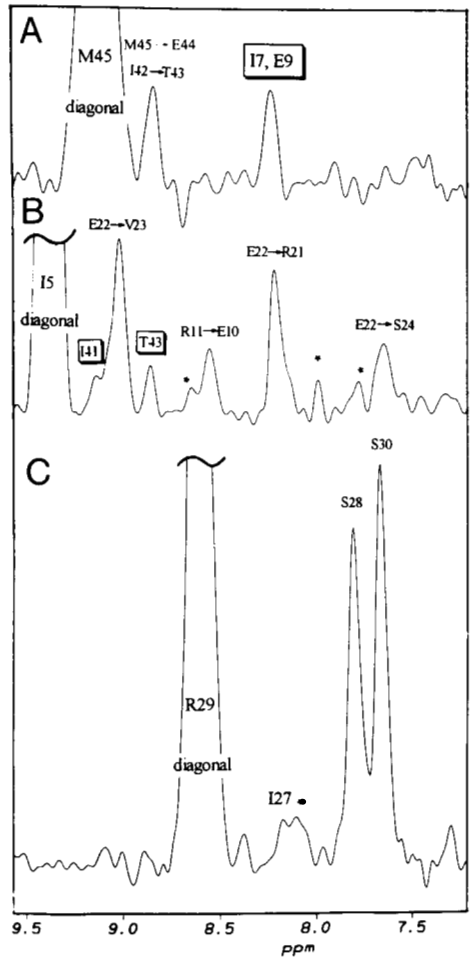

Fig. 7. F_1 slices from the 2D ^{15}N-double edited ^{1}H-NOESY spectrum of 4-OT reconstituted with only two ^{15}N-labeled subunits/hexamer (τ_{mix} = 75 ms). **A:** Slice taken at the amide proton chemical shift of Met-45, showing the cross strand HN_i-HN_j NOEs (overlapping) to Ile-7 and Glu-9 (boxed). **B:** Slice taken at the amide proton chemical shift of Ile-5 showing the cross strand NN (i, j) NOEs to Thr-43 and I-41 (boxed). **C:** Slice taken at the amide proton chemical shift of Arg-29, a residue in the helix, showing the strong NN (i, $i-1$) and NN (i, $i+1$) NOEs to Ser-28 and Ser-30 as well as the NN (i, $i-2$) NOE to Ile-27. Because this is a 2D spectrum, NOEs from other diagonal peaks with overlapping proton chemical shifts are also identified in these slices, as well as several long-range intrasubunit NOEs that have not been assigned (*). These slices were processed with a Lorentz–Gauss window function (−10 Hz, 0.05) and a cubic spline baseline correction.

Loops and turns

Two loop regions (I, residues 9–12; II, residues 34–38) are indicated by the absence of contiguous NOE correlations or chemical shift values characteristic of α-helix or β-strand structure, and fast amide exchange rates (Fig. 5). Residues Pro-34 and Leu-35 in loop II are likely to be in a region of conformational flexibility on the basis of the weak ^{1}H-^{15}N correlation for Leu-35 (Fig. 2) and the lack of intraresidue NOEs for these residues. Two turns are indicated by the NOE data. The first turn (residues 30–33), which terminates the 18-residue α-helix, is nonclassical, and the second turn (residues 47–50) is Type II′, using the criteria of Wüthrich (1986). Turn II precedes the unstable β hairpin (residues 50–57) that comprises part of the active site (see below).

β Hairpin

The NOE patterns in the region between residues 50–57 are consistent with a β hairpin structure (Figs. 5, 6), as indicated by the presence of: (1) strong αN (i, $i+1$) NOEs; (2) medium and weak cross strand NOEs, respectively, between the backbone amide protons of Ile-52 and Glu-55, and the amide protons of Phe-50 and Ala-57 in 3D ^{15}N NOESY-HSQC and 2D-^{15}N double-edited ^{1}H-NOESY spectra; (3) a strong cross strand NOE between the Hα protons of Gly-51 and Leu-56; and (4) the uniformly upfield-shifted Hα resonances.

Comparison of the NMR and crystal structure

The solution secondary structure of 4-OT determined here, and the recently solved crystal structure of a 73% identical isozyme of 4-OT (Whitman et al., 1995; Subramanya et al., 1996) are generally in good agreement.[3] The beginning and end points of the α helix, β_1 and β_2 strands, as well as the two loops and two turns, are essentially indistinguishable in both structures. However, the β hairpin seen in the crystal structure appears to be dynamic in solution (see below). This difference between the solution and crystal structure of 4-OT is significant because the β-hairpin region comprises part of the active site (see below).

The environments of the side chains of Ser-24 and Ser-30 in the crystal and NMR structures are consistent with their differing hydroxyl proton exchange behavior as found by NMR. The slowly exchanging hydroxyl proton of Ser-24 (see Table 1) may result from two factors: its location in a hydrophobic region of the α-helix, and a hydrogen bond (r = 2.8 Å) between its γ-OH and the carbonyl oxygen of residue Ile-20 as found in the crystal structure. A similar hydrogen bonding pattern has been reported previously for the slowly exchanging hydroxyl proton of Ser-56 in plastocyanin (Chazin & Wright, 1988). Consistent with these factors, in 2D NOESY spectra of 4-OT in H_2O, NOEs are observed from the γ-hydroxyl proton of Ser-24 to the $H^{\gamma Me1}$ resonance of Val-38, the $H^{\gamma Me2}$ resonance of Val-40, and the $H^{\gamma Me}$ resonance of Ile-20.

Interestingly, an equivalent hydrogen bonding interaction (r = 2.9 Å) is observed in the crystal structure of 4-OT between the γ-OH of Ser-30 and the carbonyl oxygen of Ala-26, although the γ-OH of Ser-30 is in *rapid* exchange with solvent. From the crystal structure, the side chain of Ser-30 is at the subunit interface in a less hydrophobic environment provided largely by the neighboring subunit. Hence, the faster exchange rate observed for the γ-OH of Ser-30 may reflect greater solvent accessibility at the subunit interface. In addition, because Ser-30 is the last helical residue, fraying of the helix at its carboxyl end may also contribute, as suggested by the faster amide NH exchange rate for Ser-30 relative to Ser-24 (Fig. 5).

The slowly exchanging γ-hydroxyl proton of Ser-37 in loop II (Table 1) cannot be explained by the crystal structure, because Ser-37 has been replaced by Arg and the preceding two residues differ in the isozyme studied by crystallography. It is possible

[3] Residue numbers for the isozyme studied by crystallography are increased by one unit from the numbering used here. In referring to both isozymes in the text, we use the numbering given in Table 1.

that Ser-37 is also in a hydrophobic environment because the sequence surrounding Ser-37 in the isozyme studied by NMR contains only uncharged or hydrophobic residues. In dendrotoxin K, a slowly exchanging serine residue (Ser-36) is also found in a loop and this exchange behavior has been ascribed to multiple hydrogen bond interactions (Berndt et al., 1993)

The crystal structure of 4-OT shows that the imidazole side chain of His-49, a residue located in the second turn near the active site, is solvent exposed. This is surprising because a pK_a of 5.2 for this residue was measured by proton NMR spectroscopy (Stivers et al., 1996a). This value, which is ~1.2 units lower than would be expected for a solvent-exposed histidine (Fersht, 1985), may result from the location of His-49 in the active site, which has a low dielectric constant of 22 ± 4 (Stivers et al., 1996a), and the proximity of several cationic residues (Arg-11, Arg-39, and Lys-47) as found in the crystal structure (Subramanya et al., 1996).

Oligomeric state of 4-OT

The oligomeric state of 4-OT has been suggested to be a 40.9-kDa hexamer by X-ray crystallography (Roper et al., 1994) and mass spectrometry (Fitzgerald et al., 1995). In addition, on the basis of gel filtration and ultracentrifugation studies, it was concluded that the aggregation state of 4-OT in solution was at least a pentamer (Chen et al., 1992). To test whether 4-OT was a hexamer under the conditions of the NMR experiments, dynamic light scattering measurements were performed in which the coefficient for random translational diffusion (D) is measured. The value of D can be used to calculate the molecular weight with the Svedberg equation, $M = s_{20,w}\,RT/D(1 - V\rho)$, where ρ is the density of water at 20 °C (Cantor & Schimmel, 1980), using the values determined previously for $s_{20,w} = 3.33 \times 10^{-13}$ s and partial specific volume $V = 0.729$ mL/g (Chen et al., 1992). In addition, the hydrodynamic radius (r), which is also related to the molecular size and shape, may be calculated from the diffusion coefficient using the Stokes-Einstein equation, $r = k\,T/6\pi\,\eta D$, where $\boldsymbol{k}$ is the Boltzmann constant and η is the viscosity. Using the dynamic light scattering method, 4-OT was found to be monodisperse, with $D = 8.40 \pm 0.23 \times 10^{-7}$ cm^2/s and $r = 2.99 \pm 0.08$ nm at pH 6.50 and 26 °C. This diffusion coefficient, when corrected to standard conditions of 20 °C in pure water ($D_{20,w} = 7.17 \times 10^{-7}$ cm^2/s), is in good agreement with that of other proteins of similar size (Kuntz & Kauzman, 1972; Altieri et al., 1995). Using this $D_{20,w}$, a molecular weight for 4-OT of 41.6 ± 1.1 kDa is calculated using the Svedberg equation, which agrees well with that calculated from the amino acid sequence of 4-OT (40,866), and is consistent with a hexamer in solution.[4]

The global rotational correlation time (τ_c) for 4-OT determined from both the hydrodynamic radius and NMR relaxation measurements[5] is also consistent with a hexamer in solution. We have estimated a value of 14.5 ± 1.0 ns for τ_c at pH 6.5 and 42 °C from the T_1/T_2 ratios for 18 backbone ^{15}N nuclei that did not show evidence of significant fast motion or exchange broadening (Kay et al., 1989b). This directly measured value for τ_c at 42 °C is within error of the theoretical value of 16 ± 1 ns that can be calculated using the relationship $\tau_c = 4\pi\eta r^3/3\boldsymbol{k}T$ (Cantor & Schimmel, 1980) and the hydrodynamic radius of 4-OT (see above).

Within the hexamer, subunit pairs are held together in part by the antiparallel interaction of two β_1 strands (Fig. 6). Only three such interactions are possible in the hexamer because each β_1 strand also interacts with the β_2 strand of the same subunit. Hence, the hexamer may be considered to be a trimer of dimers, consistent with the 32 symmetry of the hexamer reported in the preliminary crystal structure (Roper et al., 1994).

Identification of active site regions by transferred NOEs and affinity labeling

The complex between 4-OT and the partial substrate 2-oxo-1,6-hexanedioate (2-HD, Fig. 8) was studied by NOESY spectroscopy to identify enzyme residues within 5 Å of bound 2-HD. 4-OT catalyzes H → D exchange of the 3-protons of 2-HD, showing that 2-HD binds to the active site and is a partial substrate (Stivers et al., 1996b). A dissociation constant of 2.7 mM for the 4-OT·2-HD complex was determined from double reciprocal plots showing linear competitive inhibition by 2-HD of the isomerization of **2**.[6]

Figure 8A shows an F_2 slice from a 300 ms 2D-NOESY spectrum in H_2O of 2.72 mM 4-OT in the presence of 16.7 mM 2-HD. The slice was taken at the chemical shift of the 3-methylene protons of 2-HD (2.75 ppm), which fortuitously fall in a window where there are no overlapping resonances of the protein. The cross peak at 7.08 ppm in this slice corresponds to an intermolecular NOE from the 3-protons of 2-HD to the ϵ and/or ζ ring protons of Phe-50 (see Table 1). This intermolecular NOE was also seen as a weak cross peak (S/N = 1.75/1) in a 100-ms mixing time NOESY spectrum, and cannot be attributed to a secondary NOE via another enzymic proton, because no other NOEs from the 3-protons of 2-HD to the enzyme were seen at either mixing time. The two upfield cross peaks at 2.20 and 1.81 ppm correspond to intramolecular NOEs from the 3-protons of enzyme-bound 2-HD to its own 4- and 5-protons.

In Figure 8C is shown the F_2 slice ($\delta = 2.75$ ppm) from an identical 300-ms 2D NOESY experiment as in Figure 8A, except that 1.1 equivalents of the active site-directed affinity label 3-bromopyruvate, which selectively modifies Pro-1 (Stivers et al., 1996b), were added to displace bound 2-HD from the enzyme. In this spectrum, the NOE between 2-HD and Phe-50 is absent, and the intramolecular NOEs between the 3-, 4-, and 5-protons of 2-HD have changed in sign, as expected for a small molecule free in solution. Finally, Figure 8B shows a portion of the control spectrum of 4-OT alone; the F_2 slice taken at the same chemical shift as in Figure 8A and C shows no signal, demonstrating that the NOE to the ring protons of Phe-50 originates from the 3-protons of bound 2-HD, and not from protons of the enzyme.

[4] Hα, Cα, and amide ^{15}N line widths for 4-OT are also consistent with a hexameric structure in solution. Average values (in Hz) at 600 MHz proton frequency are: β-strands 1 and 2, Cα = 44 ± 9, Hα = 47 ± 4, ^{15}N = 16 ± 1; α helix, Cα = 38 ± 9, Hα = 35 ± 4, ^{15}N = 14 ± 1. These averages do not contain resonances that are suspected of being exchange broadened or those that show a high degree of internal mobility. The ^{15}N line widths were obtained from an ^{1}H-^{15}N HSQC spectrum recorded with a long t_1 acquisition time (0.27 s) and a final digital resolution of 0.9 Hz/point in the ^{15}N dimension. The Cα and Hα line widths were obtained from a carbonyl-coupled ^{1}H-^{13}C-CT HSQC spectrum. Errors in the line widths correspond to the respective digital resolution in the nitrogen, carbon, and proton dimensions of this spectrum.

[5] J.T. Stivers & C. Abeygunawardana (unpubl. results, 1995).

[6] C.P. Whitman (unpubl. results, 1992).

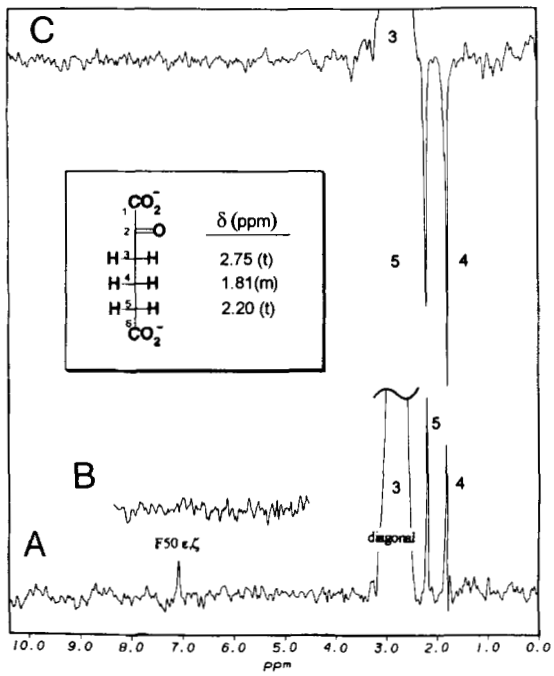

Fig. 8. Intermolecular NOEs from 4-OT to 2-oxo-1,6-hexanedioate (2-HD). F_2 rows from 600 MHz 2D NOESY spectra in H_2O of 4-OT in the presence (**A**) and absence (**B**) of 2-HD and the effects of 3-bromopyruvate (**C**) (τ_m = 300 ms, T = 42 °C). **A:** Spectrum of the 4-OT·2-HD complex taken at the chemical shift of the 3-protons of 2-HD; the NOE to the ε and/or ζ ring protons of Phe-50 is seen at 7.07 ppm. The sample contained 2.72 mM 4-OT subunits and 16.7 mM 2-HD. **B:** Spectrum of 4-OT alone; the slice was taken at the same chemical shift as in A and C, demonstrating that the NOE to the ring protons of Phe-50 originates from the 3-protons of bound 2-HD, and not from protons of the enzyme. **C:** Same as A except that 1.1 equivalents of 3-bromopyruvate were added to displace bound 2-HD from the enzyme. These slices were processed using the convolution difference routine in FELIX 1.1 to remove the residual water resonance, exponential multiplication (line broadening = 20 Hz), and a cubic spline baseline correction.

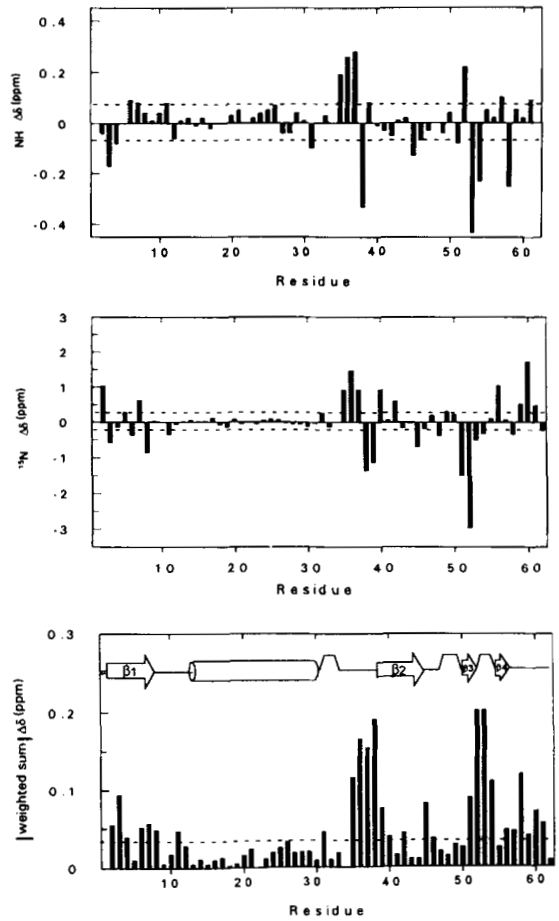

Fig. 9. Changes in backbone amide ^1H and ^{15}N chemical shifts ($\Delta\delta$) of 4-OT upon affinity labeling of Pro-1 with 3-bromopyruvate. The changes ($\Delta\delta$ = δ[unmodified] − δ[modified]) are shown as a function of the amino acid sequence of 4-OT. The bottom panel shows the sum of the absolute magnitude of nitrogen and proton chemical shift changes that were weighted according to the backbone amide chemical shift dispersion in the proton and nitrogen dimensions (2.33 ppm and 27.2 ppm, respectively). Dashed lines in each spectrum indicate the uncertainty thresholds for the $\Delta\delta$ measurements.

Thus, the above results place the ε and/or ζ protons of Phe-50 within 5 Å of the 3-protons of bound 2-HD, and indicate that Phe-50 comprises part of the active site. Accordingly, the crystal structure of 4-OT shows that the ζ carbon atom of Phe-50 is 5.4 Å from the nitrogen of Pro-1, the catalytic base, confirming that Phe-50 is in the active site, and also shows that this interaction is between subunits (Subramanya et al., 1996). Phe-50 is conserved in both isozymes of 4-OT, suggesting a role for this residue in catalysis or in structural stability. Although the quantitative effect of Phe-50 on catalysis is not known, it may contribute to the low dielectric constant of the active site, which has been estimated to be 22 ± 4 (Stivers et al., 1996a).

To further investigate regions affected by active site occupancy, the uniformly ^{15}N-labeled enzyme was reacted with the affinity label 3-bromopyruvate, which selectively modifies Pro-1 (Stivers et al., 1996b). Changes in the backbone amide ^{15}N and ^1H chemical shifts in an ^1H-^{15}N HSQC spectrum (not shown) were measured and compared to those of the unmodified enzyme (Fig. 2). A graph of the perturbations ($\Delta\delta$) in the amide ^{15}N and NH chemical shifts upon modification with 1.1 equivalents of 3-bromopyruvate (Fig. 9) reveals that the largest perturbations in ^{15}N and ^1H shifts occur for residues in the loop preceding Arg-39, and the β-hairpin following Phe-50. Significant chemical shift changes are also seen in the β_1 strand near the catalytic base, Pro-1. These chemical shift changes for loop 2 and the β-hairpin are *lower limit* values[7] because the NH chemical shift assignments of the bromopyruvate-modified

[7] Chemical shift changes were calculated by first assuming that the residue assignments were the same for all resonances in the bromopyruvate-modified enzyme, which showed no significant chemical shift changes as compared to the free enzyme. For all resonances that did show significant chemical shift changes, it was assumed that the new resonance nearest the original position was the shifted value. Thus, although the values have been interpreted conservatively as lower limits, they are still useful in revealing regions of the enzyme that undergo significant conformational changes upon ligand binding. Moreover, the largest changes are clustered together in the linear sequence of 4-OT and correlate well with more direct methods of assessing active site regions (see this paper and Stivers et al., 1996a, 1996b), providing strong evidence that the assignments are correct.

enzyme have not been made. Nevertheless, the qualitative conclusion can be made that these regions show the largest perturbations in chemical shift upon ligand binding.

A reasonable conclusion consistent with the transferred NOE and affinity labeling studies is that the active site of 4-OT is comprised of residues from loop II (34–38), the β-hairpin (50–57), as well as Pro-1. Interestingly, the β hairpin appears to be one of the most conformationally flexible regions of the free enzyme by two criteria. First, the amide hydrogen exchange rates are fast ($t_{1/2} < 30$ min), indicating that the cross strand hydrogen bonds within the β-hairpin detected in both the crystal structure (Subramanya et al., 1996) and the solution structure (Fig. 6) are frequently broken and exposed to solvent. Second, the T_1/T_2 ratios for the amide ^{15}N resonances of residues Leu-56 and Ala-57 are significantly lower than the ratios for residues in well-ordered regions of the molecule, indicating internal motions on a timescale faster than the overall correlation time.[5]

Further evidence for conformational flexibility in this region is provided by the line widths of His-49 before and after modification of Pro-1 with 3-bromopyruvate. The side-chain δ and ϵ proton resonances and ^{15}N resonances of His-49 are very broad in the free enzyme, suggestive of chemical exchange (Stivers et al., 1996b). However, upon affinity labeling of Pro-1 with 3-bromopyruvate, the δ and ϵ proton resonances of His-49 narrow selectively, as do the unassigned δ and ϵ ^{15}N resonance of a histidine residue, suggesting that His-49 adopts a more restricted conformation when a ligand is bound at the active site.

The large changes in amide ^{15}N and/or NH chemical shifts of Arg-39 and the loop preceding it after modification of Pro-1 with 3-bromopyruvate (Fig. 9) indicate a conformation change of this loop. This change in conformation may result from the direct interaction of the 1-carboxylate group of this substrate-like ligand with the guanidinium of Arg-39, the only cationic residue in this segment. It is not clear at this point whether Arg-39 also functions as the putative general acid catalyst ($pK_a = 9.0$) observed in the pH-rate profile for 4-OT (Stivers et al., 1996a). Other candidates for this role are His-49 in its neutral form and Lys-47. The pK_a values of these residues are under investigation.

Conclusions

Under NMR conditions, 4-OT was found to be a compact monodisperse hexamer. The complete secondary structure of the 4-OT subunit in the hexamer has been solved by NMR methods. It consists of a parallel $\beta_1\alpha\beta_2$ motif followed by a β-hairpin; these elements are found to be interconnected by two loops and three turns. Pairs of subunits interact to form an antiparallel β sheet between two β_1 strands, indicating that the hexamer is a trimer of dimers. These results demonstrate that, under favorable conditions (high temperature, high protein concentrations, minimal resonance overlap), the current array of heteronuclear NMR experiments can yield high quality data with proteins of ~40 kDa and τ_c values of 14.5 ns without deuterium labeling. Active site regions of 4-OT have been identified as the β_1 strand, the loop preceding Arg-39, and the β-hairpin containing Phe-50. These regions, in turn, suggest reasonable candidates for the general acid catalyst (Arg-39, His-49, and Lys-47), which functions together with Pro-1, the general-base, to bring about a 10^8-fold rate acceleration of the 4-OT reaction (Fig. 1). With all of the resonance assignments now in hand and active site regions identified, the tertiary structure, as well as the chemical and dynamic properties of active site residues, can be investigated.

Materials and methods

Materials

Crystalline 3-bromopyruvic acid was obtained from Sigma. 2-oxo-1,6-hexanedioate was synthesized as described (Nelson & Gribble, 1973). Uniformly ^{13}C-enriched glucose (99 atom %), $^{15}NH_4Cl$ (99 atom %), and ^2H_2O (99.996 atom %) were obtained from Cambridge Isotope Labs (Woburn, Massachusetts). All other solvents and reagents were of the highest quality commercially available.

4-OT sample preparation

Unlabeled, uniformly ^{15}N-labeled, and ^{13}C-^{15}N double-labeled samples of 4-OT were obtained as described previously using a T7-based expression system, except that uniformly ^{13}C-enriched glucose was substituted for glucose in the MOPS-buffered culture medium (Stivers et al., 1996b). 4-OT was purified to homogeneity as described previously (Chen et al., 1992; Stivers et al., 1996b). After eluting the enzyme from the phenyl 5-PW column, it was exchanged into 20 mM sodium phosphate buffer, pH 7.3, using an Amicon filtration cell and precipitated by adding solid ammonium sulfate to a final concentration of 3 M. The precipitate (25–80 mg) was collected by centrifugation at 20,000 × g for 30 min, dissolved in ~2 mL of water, and dialyzed twice (using 1,000 MWCO tubing) against 4 L of 6 mM potassium phosphate buffer at 4 °C, pH 6.5, containing a 0.01% (v/v) suspension of Chelex 100 to remove trace metal contaminants. The enzyme was then concentrated by lyophilization. NMR samples in 0.6 mL H_2O/D_2O (90:10) contained 3.5–7.9 mM 4-OT (in subunits), with 5–10 mM sodium phosphate buffer at pH 6.45 ± 0.05. Enzyme preparations were assayed before and after NMR experiments and, in all cases, at least 85% of the initial activity remained after prolonged studies at 42 °C. All protein concentrations are expressed in subunits.

The partially ^{15}N-labeled sample of 4-OT containing two labeled monomers/hexamer was prepared as follows. To a 0.34-mL sample of 3.96 mM unlabeled 4-OT was added 0.058 mL of a 11.6 mM solution of uniformly ^{15}N-labeled 4-OT. To this solution was added 0.6 mL of water followed by 0.48 g of solid ultrapure urea to give a final urea concentration of 6.14 M. The CD spectrum of 4-OT under these conditions indicates that the structure is random coil (not shown). After a 30-min incubation at 42 °C, the enzyme/urea solution (1.3 mL) was dialyzed at 4 °C in a 1,000 MWCO dialysis bag as described above, to remove the urea and renature the enzyme. The enzyme was lyophilized, dissolved in 0.8 mL of 90% H_2O/10% ^2H_2O, and placed in an 8-mm Shigemi small volume NMR sample tube; the final concentration of enzyme subunits was 2.55 mM, containing 33% (0.85 mM) ^{15}N-labeled subunits. Calculations assuming a Poisson distribution of labeled subunits/hexamer showed that the unwanted interactions between pairs of labeled subunits are diluted fivefold at this ratio of labeled subunits/hexamer. Control experiments verified that the enzyme activity was unaffected by these procedures, and that the ^{1}H-^{15}N HSQC spectrum for the renatured enzyme is indistinguishable from the native enzyme, both in chemical shifts and in resonance widths.

Heteronuclear NMR spectroscopy

Table 2 lists the heteronuclear and homonuclear experiments used, together with their parameters. All of the heteronuclear NMR experiments were performed on either a Varian Unityplus 500, or a Varian Unityplus 600 spectrometer equipped with z gradient capabilities, using Varian 5-mm triple resonance probes. Experiments with the partially ^{15}N-labeled enzyme sample were done at 600 MHz with a Nalorac 8-mm triple resonance probe equipped with a z gradient coil. Pulse sequences, modified to include pulsed field gradients and water flip-back pulses, were employed in all of the experiments in order to minimize artifacts due to pulse imperfections and to reduce the saturation of the water resonance (Bax & Pochapsky, 1992; Muhandiram & Kay, 1994). All experiments were performed with the proton carrier centered on the water frequency (4.61 ppm) in all ^{1}H dimensions, unless noted otherwise in Table 2. Data were processed on a Silicon Graphics Personal IRIS 4D/35 Workstation using the FELIX software package (Biosym Technologies, Inc.). Unless otherwise noted, multidimensional data sets were collected using the States–TPPI method (Marion et al., 1989) in all the indirect dimensions, with relaxation delays of 0.9 s. These acquired time domain data points were extended by one-third of the original size by the forward linear prediction routine in FELIX. Shifted (65°–90°) sine bell filters were used in the first and subsequent dimensions, respectively, prior to zero-filling and Fourier transformation.

2D Homonuclear NMR experiments

All of the homonuclear NMR experiments (Table 2) were performed on a Bruker AM600 NMR spectrometer. To identify residues of 4-OT within proximity of the bound partial substrate 2-oxo-1,6-hexanedioate, 2D NOESY spectra with mixing times of 100 and 300 ms were acquired (Table 2). The sample contained 2.72 mM 4-OT, 16.7 mM 2-oxo-1,6-hexanedioate, and 10 mM sodium phosphate, pH 7.00, in 90% H_2O/10% ^2H_2O in a total volume of 0.495 mL. To assign the cross strand H_α NOEs in the β-strand structure of 4-OT, 2D NOESY spectra (Kumar et al., 1980) in ^2H_2O were acquired with 30-ms, 50-ms, and 100-ms mixing times (Table 2). The sample contained 3.2 mM 4-OT.

The observed ^{1}H chemical shifts are reported with respect to either the H_2O or HOD signal, which is 4.61 ppm downfield from external TSP at 42 °C. To insure identical sample temperatures between different spectrometers, the temperature settings were adjusted to yield a chemical shift separation of 4.61 ppm between the HOD and TSP lines in a sample of TSP in ^2H_2O.

Table 2. *Summary description of the heteronuclear and homonuclear NMR experiments used to determine the solution structure and substrate interactions of 4-oxalocrotonate tautomerase*[a]

Experiment and pulse sequence	Transients	Acquired data (complex points)			Sweep widths (Hz)			Matrix size (real points)		
	fid	t_1	t_2	t_3	ω_1	ω_2	ω_3	ω_1	ω_2	ω_3
^{15}N-HSQC[b]	4	192 (N)	1,024 (H)		1,600	8,000		1,024	1,024	
^{15}N-TOCSY-HSQC[c]	8	92 (H)	32 (N)	1,280 (H)	4,800	1,885	10,000	512	128	512
^{15}N-NOESY-HSQC[d]	4, (8)[e]	128 (H)	48 (N)	1,024 (H)	6,400	1,885	8,000	256	128	512
^{15}N-HMQC-NOESY-HSQC[f]	8	32 (N)	42 (N)	1,280 (H)	1,800	1,800	10,000	128	128	512
^{15}N-double-edited ^{1}H-NOESY[g]	1152	64 (H)	1,024 (H)		2,000	8,000		512	512	
^{13}C CT-HSQC[h]	64	216 (C)	1,024 (H)		9,052	8,000		1,024	1,024	
CT HNCA[i]	32	48 (N)	30 (C)	1,024 (H)	4,200	1,509	8,000	128	256	256
HNCACB[j]	32	48 (N)	32 (C)	1,024 (H)	7,200	2,000	8,000	128	256	256
CT HNCO[k]	8	48 (N)	32 (C)	1,024 (H)	4,200	1,509	8,000	128	256	256
HCCH-TOCSY[l]	64	96 (H)	26 (C)	960 (H)	3,500	3,000	8,000	256	64	512
^{1}H-NOESY[m]	32, (64)[n]	512 (H)	2,048 (H)		6,944	7,246		2,048	1,024	

[a] ^{15}N-HSQC, 100-ms ^{15}N-NOESY-HSQC, and HCCH-TOCSY experiments were done at 500 MHz; all others were done at 600 MHz (proton frequency). Digital resolution in the directly detected ^{1}H dimension was ≤0.013 ppm/point for all experiments.

[b] Bodenhausen and Ruben (1980). The pulse sequence of Mori et al. (1995) was used to avoid water excitation; the nitrogen carrier was centered at 120 ppm.

[c] Marion et al. (1989).

[d] Kay et al. (1989a).

[e] Two experiments with mixing times of 50 and 100 ms were performed; 4 and 8 transients/fid were collected, respectively.

[f] Ikura et al. (1990a). Mixing time was 50 ms.

[g] Otting and Wüthrich (1990). The ω_2 half-filter was achieved by the water flip-back HSQC sequence of Mori et al. (1995); mixing time was 75 ms. For t_1, the ^{1}H carrier frequency was centered at 8.12 ppm.

[h] Vuister and Bax (1992); Kay et al. (1992); carbon pulses were applied with a 10.7-kHz RF field centered at 42 ppm and ^{13}C decoupling during acquisition was achieved with a 4-kHz RF field.

[i] Grzesiek and Bax (1992); Kay et al. (1992).

[j] Wittekind and Mueller (1993); Kay et al. (1992).

[k] Ikura et al. (1990b); Kay et al. (1992).

[l] Bax et al. (1990); position of the carrier frequencies during frequency labeling were 2.91 ppm (H), 43 ppm (C), and 4.61 ppm (H) during t_1, t_2, and t_3, respectively. Three cycles of DIPSI-3 mixing (20.5 ms, 8-kHz field) were used.

[m] Marion and Wüthrich (1983); Kumar et al. (1980). NOESY spectra (in ^2H_2O) had mixing times of 30, 50, 100 ms.

[n] Transferred NOE experiments were done with two mixing times of 100 and 300 ms, with 64 transients/fid and a final matrix size of 2K × 2K.

The carbon chemical shifts are reported with respect to external TSP in ^2H_2O (0.0 ppm). The nitrogen chemical shifts are reported with respect to external $^{15}NH_4Cl$ (2.9 mM in 1 M HCl) at 20 °C, which is 24.93 ppm downfield from liquid NH_3 (Levy & Lichter, 1979).

Dynamic light scattering measurements

The diffusion coefficient (D) for hexameric 4-OT was measured using a 2 mg/mL protein solution in 10 mM sodium phosphate buffer at pH 6.5 and 26 °C using a DP-801 dynamic light scattering instrument (Protein Solutions, Inc.). Before injection, the solution was filtered through a 20-nm syringe filter. Ten independent measurements of D were made, from which the average value and standard error were calculated. The hydrodynamic radius (r) was calculated from the average D value using the Stokes–Einstein equation (which assumes a spherical molecule), and the viscosity of pure water at 26 °C ($\eta = 8.705 \times 10^{-3}$ g s^{-1} cm^{-1}). There is no significant difference between the viscosity of pure water and the dilute protein and buffer solution used in this experiment.

Acknowledgments

We are grateful to Dr. Cynthia Wolberger for permission to use her dynamic light scattering instrument and to Stephen Soisson and Qinjian Zhao for advice on its use. This work was supported by National Institutes of Health grant DK28616 (to A.S.M.) and the American Chemical Society Petroleum Research Fund grant 28020-AC4 (to C.P.W.). J.T.S. is an American Cancer Society Postdoctoral Fellow.

References

Abeygunawardana C, Weber DJ, Frick DN, Bessman MJ, Mildvan AS. 1993. Sequence specific assignments of the backbone ^1H, ^{13}C, and ^{15}N resonances of the Mut T enzyme by heteronuclear multidimensional NMR. *Biochemistry 32*:13071–13080.

Abeygunawardana C, Weber DJ, Gittis AG, Frick DN, Lin J, Miller AF, Bessman MJ, Mildvan AS. 1995. Solution structure of the Mut T enzyme, a nucleoside pyrophosphohydrolase. *Biochemistry 34*:14997–15005.

Alteiri AS, Hinton DP, Byrd RA. 1995. Association of biomolecular systems via pulsed field gradient NMR self-diffusion measurements. *J Am Chem Soc 117*:7566–7567.

Bax A, Clore GM, Gronenborn AM. 1990. ^1H-^1H correlation via isotropic mixing of ^{13}C magnetization, a new 3D approach for assigning ^1H and ^{13}C spectra of ^{13}C-enriched proteins. *J Magn Reson 88*:425–431.

Bax A, Grzesiek S. 1993. Methodological advances in protein NMR. *Accts Chem Res 26*:131–138.

Bax A, Pochapsky SS. 1992. Optimized recording of heteronuclear multidimensional NMR spectra using pulsed field gradients. *J Magn Reson 99*:638–643.

Bayley RC, Barbour MG. 1984. *Microbiological degradation of organic compounds*. New York: Marcel Dekker. pp 253–294.

Berndt KD, Beunink J, Schröder W, Wüthrich K. 1993. Designed replacement of an internal hydration molecule in BPTI: Structural and functional implications of a glycine-to-serine mutation. *Biochemistry 32*: 4564–4570.

Bodenhausen G, Ruben DJ. 1980. Natural abundance ^{15}N NMR by enhanced heteronuclear NMR spectroscopy. *Chem Phys Lett 69*:185–188.

Cantor CR, Schimmel PR. 1980. *Biophysical chemistry*. New York: W.H. Freeman.

Chazin WJ, Wright PE. 1988. Complete assignment of the ^1H nuclear magnetic resonance spectrum of French bean plastocyanin. *J Mol Biol 202*:623–636.

Chen LH, Kenyon GL, Curtin F, Harayama S, Bembenek ME, Hajipour G, Whitman CP. 1992. 4-oxalocrotonate tautomerase, an enzyme composed of 62 amino acid residues per monomer. *J Biol Chem 267*:17716–17721.

Clore GM, Omichinski JG, Sakaguchi K, Zamrano N, Sakamoto H, Apella E, Gronenborn AM. 1994. High resolution structure of the oligomerization domain of p53 by multidimensional NMR. *Science 265*:386–391.

Clore GM, Omichinski JG, Sakaguchi K, Zamrano N, Sakamoto H, Apella E, Gronenborn AM. 1995. Interhelical angles in the solution structure of the oligomerization domain of p53:correction. *Science 267*:1515–1516.

Clubb RT, Omichinski JG, Sakaguchi K, Apella E, Gronenborn AM, Clore GM. 1995. Backbone dynamics of the oligomerization domain of p53 determined from ^{15}N NMR relaxation measurements. *Protein Sci 4*: 855–862.

Englander SW, Kallenbach NR. 1984. Hydrogen exchange and structural dynamics of proteins and nucleic acids. *Quart Rev Biophys 16*:521–655.

Fersht A. 1985. *Enzyme structure and mechanism*. New York: W.H. Freeman.

Fitzgerald MC, Chernushevich I, Standing KG, Kent SBH, Whitman C. 1995. Total chemical synthesis and catalytic properties of the enzyme enantiomers L- and D-4-oxalocrotonate tautomerase. *J Am Chem Soc 117*: 11075–11080.

Fogh RH, Schipper D, Boelens R, Kaptein R. 1994. ^1H, ^{13}C and ^{15}N NMR backbone assignments of the 269-residue serine protease PB92 from *Bacillus alcalophilus*. *J Biomol NMR 4*:123–128.

Gagné SM, Tsuda S, Li MX, Chandra M, Smillie LB, Sykes BD. 1994. Quantification of the calcium-induced secondary structural changes in the regulatory domain of troponin C. *Protein Sci 3*:1961–1974.

Gerlt JA, Gassman PG. 1993. An explanation for the rapid proton abstraction from carbon acids: Importance of late transition states in concerted mechanisms. *J Am Chem Soc 115*:11552–11568.

Grzesiek S, Bax A. 1992. Improved 3D triple-resonance NMR techniques applied to a 31 kDa protein. *J Magn Reson 96*:432–440.

Grzesiek S, Dobeli H, Gentz R, Garotta G, Labhardt AM, Bax A. 1992. ^1H, ^{13}C, and ^{15}N NMR backbone assignments and secondary structure of human interferon γ. *Biochemistry 31*:8180–8190.

Ikura M, Bax A, Clore GM, Gronenborn AM. 1990a. Detection of nuclear Overhauser effects between degenerate amide proton resonances by heteronuclear three-dimensional nuclear magnetic resonance spectroscopy. *J Am Chem Soc 112*:9020–9022.

Ikura M, Kay LE, Bax A. 1990b. A novel approach for sequential assignment of ^1H, ^{13}C, and ^{15}N spectra of larger proteins: Heteronuclear triple-resonance three-dimensional NMR spectroscopy. Application to calmodulin. *Biochemistry 29*:4659–4667.

Kay LE, Keifer P, Saarinen T. 1992. Pure absorption gradient enhanced heteronuclear single quantum coherence spectroscopy with improved sensitivity. *J Am Chem Soc 114*:10663–10665.

Kay LE, Marion D, Bax A. 1989a. Practical aspects of 3D heteronuclear NMR of proteins. *J Magn Reson 84*:72–84.

Kay LE, Torchia DA, Bax A. 1989b. Backbone dynamics of proteins as studied by ^{15}N inverse detected heteronuclear NMR spectroscopy: Application to staphylococcal nuclease. *Biochemistry 28*:8972–8979.

Kumar A, Wagner G, Ernst RR, Wüthrich K. 1980. Studies of J-connectivities and selective ^1H-^1H Overhauser effects in H_2O solutions of biological macromolecules by two dimensional NMR experiments. *Biochem Biophys Res Commun 96*:1156–1163.

Kuntz ID, Kauzman W. 1972. Hydration of proteins and polypeptides. *Adv Prot Chem 28*:236–345.

Levy GC, Lichter RL. 1979. *Nitrogen-15 NMR spectroscopy*. New York: John Wiley and Sons Inc.

Marion D, Driscoll PC, Kay LE, Wingfield PT, Bax A, Gronenborn AM, Clore GM. 1989. Overcoming the overlap problem in the assignment of ^1H NMR spectra of larger proteins by use of three dimensional heteronuclear ^1H-^{15}N Hartmann–Hahn multiple quantum coherence and nuclear Overhauser multiple quantum coherence spectroscopy: Application to interleukin 1β. *Biochemistry 28*:6150–6156.

Marion D, Wüthrich K. 1983. Application of phase sensitive two dimensional correlated spectroscopy (COSY) for measurements of ^1H-^1H spin-spin coupling constants in proteins. *Biochem Biophys Res Commun 113*: 967–974.

Mori S, Abeygunawardana C, Johnson MO, van Zijl PCM. 1995. Improved sensitivity of HSQC spectra of exchanging protons at short interscan delays using a new fast HSQC (FHSQC) detection scheme that avoids water saturation. *J Magn Reson 108B*:94–98.

Muhandiram DR, Kay LE. 1994. Gradient enhanced triple resonance three dimensional NMR experiments with improved sensitivity. *J Magn Reson 103B*:203–216.

Nelson RB, Gribble GW. 1973. On the preparation of α-ketoadipic acid. *Organic Preparations and Procedures Int 5*:55–58.

Otting G, Wüthrich K. 1990. Heteronuclear filters in 2D[^1H,^1H]NMR spectroscopy: Combined use with isotopic labeling for studies of macromolecular conformation and intermolecular interactions. *Quart Rev Biophys 23*:39–96.

Roper DJ, Subramanya HS, Shingler V, Wigley DB. 1994. Preliminary crystallographic analysis of 4-oxalocrotonate tautomerase reveals the oligomeric structure of the enzyme. *J Mol Biol 243*:799–801.

Spera S, Bax A. 1991. Empirical correlation between protein backbone conformation and Cα and Cβ NMR chemical shifts. *J Am Chem Soc 113*: 5490–5492.

Spera S, Ikura M, Bax A. 1991. Measurement of the exchange rates of rapidly exchanging amide protons: Application to the study of calmodulin and its complex with myosin light chain kinase fragment. *J Biomol NMR 1*:155–165.

Stivers JT, Abeygunawardana C, Mildvan AS, Hajipour G, Whitman CP. 1996a. 4-Oxalocrotonate tautomerase: pH dependence of catalysis and pK_a values of active site residues. *Biochemistry 35*:814–823.

Stivers JT, Abeygunawardana C, Mildvan AS, Hajipour G, Whitman CP, Chen LH. 1996b. The catalytic role of the amino-terminal proline in 4-oxalocrotonate tautomerase: Affinity labeling and heteronuclear NMR studies. *Biochemistry 35*:803–813.

Stivers JT, Abeygunawardana C, Whitman CP, Mildvan AS. 1995. Sequence specific NMR assignments and solution secondary structure of 4-oxalocrotonate tautomerase, a 41 kDa homohexamer. San Francisco, California: *ASBMB/DBC-ACS Meeting*. [Late Breaking Abstracts: Abstr. LB70].

Subramanya HS, Roper DI, Dauter Z, Dodson EJ, Davies GJ, Wilson KS, Wigley DB. 1996. Enzymatic ketonization of 2-hydroxymuconate: Specificity and mechanism investigated by the crystal structures of two isomerases. *Biochemistry 35*:792–802.

Vuister GW, Bax A. 1992. Resolution enhancement and spectral editing of uniformly ^{13}C enriched proteins by homonuclear broad band ^{13}C decoupling. *J Magn Reson 98*:428–435.

Whitman CP, Hajipour G, Watson RJ, Johnson WH Jr, Bembenek ME, Stolowich NJ. 1992. Stereospecific ketonization of 2-hydroxymuconate by 4-oxalocrotonate tautomerase and 5-carboxymethyl-2-hydroxymuconate isomerase. *J Am Chem Soc 114*:10104–10110.

Whitman CP, Wigley DB, Johnson W, Hajipour G. 1995. Inactivation of 4-oxalocrotonate tautomerase by 2-oxo-4-pentynoate implicates the N-terminal proline as the catalytic base. *FASEB J 9*:A1482. [Abstr. 1306].

Wishart DS, Sykes BD, Richards FM. 1991. Relationship between NMR chemical shift and protein structure. *J Mol Biol 222*:311–333.

Wishart DS, Sykes BD, Richards FM. 1992. The chemical shift index: A fast and simple method for the assignment of protein secondary structure through NMR spectroscopy. *Biochemistry 31*:1647–1651.

Wittekind M, Mueller L. 1993. HNCACB, a high sensitivity 3D NMR experiment to correlate amide-proton and nitrogen resonances in proteins. *J Magn Reson 101B*:201–205.

Wüthrich K. 1986. *NMR of proteins and nucleic acids*. New York: J. Wiley & Sons, Inc. pp 162–175.

Xue L, Mildvan AS, Talalay P. 1990. Studies of the mechanism of the Δ^5-3-ketosteroid isomerase reaction by substrate, solvent, and combined kinetic deuterium isotope effects on wild-type and mutant enzymes. *Biochemistry 29*:7491–7500.

Yamazaki T, Lee W, Arrowsmith CH, Muhandiram DR, Kay LE. 1994. A suite of triple resonance NMR experiments for the backbone assignment of ^{15}N ^{13}C, ^{2}H labeled proteins with high sensitivity. *J Am Chem Soc 116*:11655–11666.